

NASA TECHNICAL NOTE



NASA TN D-3

LOAN COPY: RET
AFWL (WLI)
KIRTLAND AFB,

CAPE-
pt. 2
c.1



TECH LIBRARY KAFB, NM

0067259

NASA TN D-3368

COLD-AIR PERFORMANCE EVALUATION OF SCALE MODEL OXIDIZER PUMP-DRIVE TURBINE FOR THE M-1 HYDROGEN-OXYGEN ROCKET ENGINE

II - OVERALL TWO-STAGE PERFORMANCE

by Richard J. Roelke, Roy G. Stabe, and David G. Evans

Lewis Research Center

Cleveland, Ohio





0067259

NASA TN D-3368

COLD-AIR PERFORMANCE EVALUATION OF SCALE MODEL
OXIDIZER PUMP-DRIVE TURBINE FOR THE M-1
HYDROGEN-OXYGEN ROCKET ENGINE
II - OVERALL TWO-STAGE PERFORMANCE

By Richard J. Roelke, Roy G. Stabe, and David G. Evans

Lewis Research Center
Cleveland, Ohio

NATIONAL AERONAUTICS AND SPACE ADMINISTRATION

For sale by the Clearinghouse for Federal Scientific and Technical Information
Springfield, Virginia 22151 - Price \$0.50

COLD-AIR PERFORMANCE EVALUATION OF SCALE MODEL OXIDIZER PUMP-DRIVE TURBINE FOR THE M-1 HYDROGEN-OXYGEN ROCKET ENGINE

II - OVERALL TWO-STAGE PERFORMANCE

by Richard J. Roelke, Roy G. Stabe, and David G. Evans

Lewis Research Center

SUMMARY

The aerodynamic performance of a 0.45-scale model of the oxidizer pump-drive turbine and inlet manifold assembly for the M-1 rocket engine was experimentally evaluated with air at ambient inlet conditions. Speed was varied from 60 to 110 percent of equivalent design speed for equivalent pressure ratios ranging from 1.3 to 2.8.

At equivalent design speed and pressure ratio, the turbine static efficiency was 0.524 and the equivalent specific work was 9.61 Btu per pound compared with the design values of 0.536 and 9.832 Btu per pound, respectively. The turbine equivalent weight flow was 10.8 percent less than design. Of this deficit, 3.7 percent was attributed to an undersize nozzle throat area of the test hardware, and the remaining part was charged to adverse flow conditions in the inlet manifold and nozzle channels. The result of these deviations from design was a net loss of 12.8 percent in turbine power at design speed and pressure ratio.

Radial surveys taken at the turbine exit at design equivalent speed and pressure ratio revealed circumferential and radial variations in total pressure similar in pattern but attenuated from those measured in prior inlet manifold surveys. Also observed was overturning of the flow and large circumferential variations in absolute flow angle, both of which occurred at all but the tip region of the blade passage. In the tip region, flow velocities lower than design existed, which lead to significant underturning of the flow.

Static-pressure measurements taken on each side of the rotor disks below the hub indicated shaft thrusts considerably higher than anticipated.

INTRODUCTION

The aerodynamic performance evaluation of the pump-drive turbines for the M-1

engine has been included as part of the turbine research and project support program. The M-1, a 1.5-million-pound-thrust hydrogen-oxygen rocket engine, utilizes separate fuel and oxidizer turbines in series with a single gas generator supplying the driving gas. The approach used in the design of the turbines was that of simplicity, light weight, and reasonable efficiency. These considerations led to the use of two-stage velocity-compounded cantilevered turbines for both pump drives.

The aerodynamic design of the oxidizer pump-drive turbine (oxidizer turbine, Model III) is reported in reference 1. The design of the turbine and the turbine blading was unusual in several aspects. The requirements imposed on the turbine by the turbopump system were those of low rotative speed and high propellant energy. These requirements resulted in a very low blade-jet speed ratio for a two-stage turbine of only 0.128. Further, in order to simplify construction, identical blade profiles with blunt leading edges were incorporated for both rotors and the second-stage stator; however, the blade rows had different stagger angles.

The aerodynamic performance of a 0.45-scale feedpipe-manifold portion of the turbine with the nozzle in place was evaluated with air at approximately ambient inlet conditions and is reported in reference 2. The investigation indicated that as a result of minimizing flow areas in the feedpipes and manifold with attendant increases in flow Mach number, severe maldistribution of the flow existed which nearly doubled the predicted loss in feedpipe dynamic pressure and substantially reduced the flow capacity of the nozzle from that used in the design.

The results of the cold-air experimental evaluation of the complete turbine are presented herein. The performance of the 0.45-scale turbine was obtained for a range of total- to static-pressure ratios from 1.3 to 2.8 and speeds from 60 to 110 percent of equivalent design speed. In addition, zero speed torque for the same range of pressure ratios was also measured. Also included is a brief description of the M-1 turbopump system and oxidizer turbine as well as the scale test turbine, test facility, and procedures used in the evaluation.

SYMBOLS

\mathcal{A}	aspect ratio, h/c
c	blade chord (max. x value, table V), in.
c_p	specific heat at constant pressure, $\text{Btu}/(\text{lb})(^\circ\text{R})$
g	gravitational constant, $32.17 \text{ ft}/\text{sec}^2$
h	blade height, in.
Δh	specific work, Btu/lb

J	mechanical equivalent of heat, 778 ft-lb/Btu
N	rotative speed, rpm
P	power, hp
p	absolute pressure, lb/sq in. abs
R	gas constant, ft-lb/(lb)(°R)
r	radius, in.
s	blade pitch, in.
T	absolute temperature, °R
U	blade speed, ft/sec
V	absolute gas velocity, ft/sec
W	gas velocity relative to blade, ft/sec
w	weight flow, lb/sec
γ	ratio of specific heats
δ	ratio of inlet total pressure to NACA standard sea-level pressure, $p'_1/14.696$
ϵ	function of γ used in relating weight flow and torque to those using inlet conditions at NACA standard sea-level atmosphere, $\frac{0.740}{\gamma} \left(\frac{\gamma + 1}{2} \right)^{\gamma/(\gamma-1)}$
η	static efficiency, based on total- to static-pressure ratio across turbine
θ_{cr}	squared ratio of turbine-inlet critical velocity to that of NACA standard sea-level atmosphere, $\left(\frac{V_{cr, 1}}{1019.46} \right)^2$
ν	blade-jet speed ratio, $U_m / \sqrt{2gJc_p T'_1 \left[1 - \left(\frac{p_{7,w}}{p'_1} \right)^{(\gamma-1)/\gamma} \right]}$

Subscripts:

cr	conditions corresponding to Mach number of 1
h	blade hub section
m	blade mean section
p	measuring probe
t	blade tip section

w	exhaust pipe wall
1, 2, 3, 4, 5, 6, 7	measuring stations (see fig. 7)
ϕ	measured at center of feedpipe, station 1
Superscripts:	
—	average
'	absolute total state

TURBOPUMP SYSTEM

A mockup of the M-1 engine turbopump feed system and a portion of the expansion nozzle is presented in figure 1. Figure 1(a) shows the separate fuel and oxidizer turbopumps mounted on either side of the engine combustion chamber. A single gas generator supplies the turbines with the fuel-rich combustion products of liquid hydrogen and liquid oxygen. These combustion gases are discharged into the fuel turbine manifold, are expanded in the turbine, and are conveyed to the oxidizer turbine by two crossover ducts. The ends of the crossover ducts entering the oxidizer turbine manifold are referred to herein as the "feedpipes." After passing through the oxidizer turbine manifold, the gases are expanded through the turbine into a hemispherically shaped exhaust housing (fig. 1(b)), are passed through the nozzle skirt coolant passages, and are then expanded overboard through choked nozzles to supplement engine thrust. Figure 2 shows the internal arrangement of the turbine components within the turbopump assembly, from which the compact, cantilevered design can be noted.

TURBINE DESCRIPTION

The following oxidizer turbine description is divided into three parts. The overall design requirements and velocity diagrams are presented first, followed by a general description of the turbine hardware and blading design characteristics. The remaining part includes a discussion of some of the similarity considerations made between the scale and the full-size machines and concludes with a brief description of the test unit.

Overall Requirements

The turbine is a two-stage velocity-compounded machine with a nominally constant

TABLE I. - TURBINE DESIGN REQUIREMENTS

Parameter	Combustion products of hydrogen and oxygen	NACA standard inlet air equivalent conditions	
		Full size	0.45 Scale
Turbine power, hp	^a 29 120	485.6	98.33
Weight flow, lb/sec	115	34.92	7.071
Rotative speed, rpm	3635	852	1893
Specific work, Btu/lb	^a 179.0	9.832	9.832
Inlet total temperature, T_1^* , °R	1190	518.7	518.7
Inlet total pressure, p_1^* , lb/sq in. abs	208.1	14.696	14.696
Pressure ratio, $p_1^*/p_{7,w}$	^b 1.738	^b 1.745	^b 1.745
Static efficiency, η	^b 0.536	^b 0.536	^b 0.536
Blade-jet speed ratio, ν	^b 0.128	^b 0.128	^b 0.128

^aComputed from velocity diagrams.

^bCorrected to rating stations other than those used in refs.

1 and 2; see DATA REDUCTION.

TABLE II. - GAS PROPERTIES

Gas	Combustion products of hydrogen and oxygen	NACA standard air
Specific heat, c_p , Btu/(lb)(°R)	1.98	0.241
Gas constant, R , ft-lb/(lb)(°R)	425.8	53.35
Ratio of specific heats, γ	1.382	1.40

TABLE III. - DESIGN STATIC PRESSURE DISTRIBUTION

Blade row	Pressure, lb/sq in. abs					
	Inlet			Exit		
	Hub	Mean	Tip	Hub	Mean	Tip
Nozzle	200	200	200	115.5	126.8	136
First-stage rotor	115.5	126.8	136	119.2	126.8	132.2
Second-stage stator	119.2	126.8	132.2	115	124.8	132.2
Second-stage rotor	115	124.8	132.2	115	120	124.4

mean diameter of 33 inches. The turbine aerodynamic design specifications are listed in table I, and the gas properties of the hydrogen-oxygen combustion products corrected from those used in the design, along with NACA standard-air conditions, are listed in table II.

The design free-stream mean-diameter velocity diagrams needed to satisfy the preceding requirements and a specified work split of 63 and 37 percent between the first and second stages, respectively, are shown in figure 3. All velocities in the turbine were subsonic. Also to be noted from the figure is the relatively high amount of exit whirl, 56.5° . The design static pressure distribution through the turbine is given in table III.

Turbine Geometry

A cross-sectional view of the oxidizer turbine, Model III, is presented in figure 4(a).

TABLE IV. - BLADE DESIGN CHARACTERISTICS

Blade row	Flow channel turning, deg	Radius ratio, r_h/r_t	Aspect ratio, A	Solidity, $(c/s)_m$	Number of blades
Nozzle	70	0.823	0.85	1.57	43
First-stage rotor	134.7	.789	2.26	1.63	98
Second-stage stator	130.1	.746	2.78	1.62	97
Second-stage rotor	125.6	.711	3.21	1.57	94

The flight hardware was designed with a spherically shaped outer casing structure that includes the inlet manifold and exhaust section. The centerlines of the two feedpipes entering the manifold form an angle of 80° . In each of these feedpipes, there is a flow deflector plate to prevent the flow from impinging directly onto the nozzle tip wall that is in line with the feedpipe.

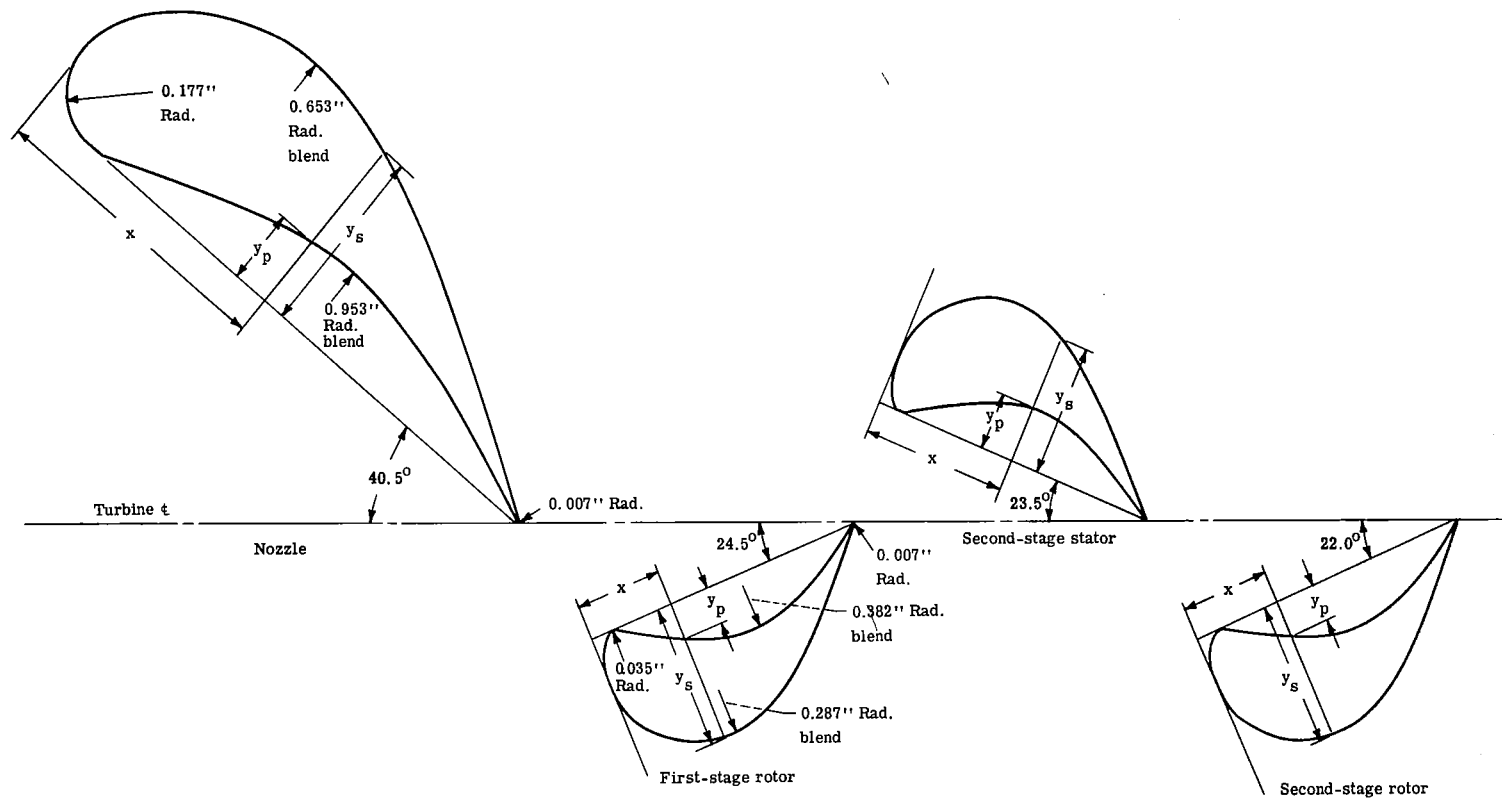
All blades of the turbine were constant-section nontwisted designs with a curved suction surface downstream of the throat. Identical blade profiles with blunt leading edges were utilized for the rotors and the second-stage stator. The turbine flow areas of successive blade rows were increased by increasing the blade heights and changing the blade stagger angles. The general characteristics of the four blade rows are given in table IV.

Scale Test Unit

The oxidizer turbine test unit was built to 0.45 of full scale to adapt it to an existing cold-air test facility. This change in scale and working fluid of the model turbine resulted in a turbine Reynolds number of only one-tenth of the design Reynolds number for the actual oxidizer turbine. The design Reynolds number of the full-size hot turbine was 7×10^6 , whereas the range of values for the model turbine operating with ambient air was between 6.2×10^5 and 8.3×10^5 for the range of pressure ratios covered. Even with this large change in Reynolds number, however, the Reynolds number of the model turbine was considerably above the value indicated in reference 3 at which any significant effect on performance would be expected.

A cross section of the test unit is shown in figure 4(b). Some deviations from exact similarity between the scale and the full-size turbines were permitted to simplify manufacture. The hemispherically shaped exhaust section with the two exhaust ducts of the full-size turbine was not included in the evaluation but was replaced with a conically shaped single exhaust pipe. Also, the cross-sectional shapes of the inlet manifold of the two turbines differed slightly; however, the scaled manifold flow area was maintained in the test unit. A comparison of figures 4(a) and (b) illustrates these differences.

TABLE V. - TEST TURBINE BLADE COORDINATES



Nozzle coordinates		
x, in.	y _s , in.	y _p , in.
0.000	0.177	0.177
.100	.390	.020
.200	.475	.002
.300	.525	.041
.400	.555	.078
.500	.563	.118
.600	.558	.150
.800	.507	.200
1.000	.423	.208
1.200	.319	.175
1.400	.200	.115
1.600	.078	.041
1.703	.007	.007

Stator and rotor coordinates		
x, in.	y _s , in.	y _p , in.
0.000	0.135	0.135
.010	.210	.060
.025	.250	.030
.050	.285	.005
.100	.333	.022
.150	.363	.055
.200	.380	.083
.300	.383	.128
.400	.347	.150
.500	.278	.143
.600	.190	.107
.700	.090	.055
.778	.007	.007

The coordinates of the scale blade profiles are given in table V. A discrepancy of the scale blading from the specification resulted during the manufacture of the test unit. In general, the channel throat heights and widths were made less than the design dimensions; the following undersize throat areas resulted:

Blade row	Amount that throat area was undersize from design, percent
Nozzle	3.7
First-stage rotor	9.0
Second-stage stator	4.2
Second-stage rotor	5.2

It was recognized that these deficiencies in the flow areas prevented exact simulation of the full-size turbine geometry and had probable effects on the turbine flow conditions. They were judged to be of insufficient magnitude, however, to affect the general level of overall performance appreciably.

Figure 5 shows partial assemblies of the scale hardware prior to testing. In figure 5(a) is the downstream end of the nozzle installed in the feedpipe-manifold assembly. The figure also shows the angle (80°) formed by the two feedpipes. Figure 5(b) presents the second-stage rotor prior to installation of the tip shroud. The blade profile, which is representative for both rotors as well as for the second-stage stator, can be noted. Figure 5(c) illustrates the split casing designed for the scale test unit, with the second-stage stator installed. An assembly of the manifold, lower casing half, and shrouded rotors is shown in figure 5(d). The inlet header which supplies the air to the two feedpipes and the scale turbine casing mounted on a support stand are presented in figure 5(e). The similarity in flow areas between the full-size and the scale turbine begins at the point at which the feedpipe diameter is reduced just prior to the entrance to the manifold and terminates at the trailing edge of the second-stage rotor.

APPARATUS AND INSTRUMENTATION

Test Facility

The test facility used in the experimental investigation was the same as that of reference 2. Figure 6 shows the arrangement of the equipment in the test cell. In operation, dry air from the laboratory high-pressure-air system flows through the inlet ducting, a calibrated orifice, and an automatic pressure control valve and into the test unit through an 8-inch-diameter header connecting the two feedpipes. After expanding through the

turbine, the air is discharged through the exhaust-pipe control valve to the laboratory altitude-exhaust system.

Turbine output power was transmitted through a cradled gear box and absorbed by a cradled direct-current electric dynamometer, which also served as a speed control. The total reaction torque of the gear box and the dynamometer was measured with a single self-balancing pneumatic torque cell.

Instrumentation

The axial and circumferential locations of the instrumentation within the test turbine are shown in figure 7. Overall turbine performance was calculated from measurements taken at stations 1 and 7. The flow conditions in each feedpipe (station 1) were measured with four static pressure taps, one shielded total-pressure probe and two thermocouples. The instrumentation installed at station 7 consisted of four static-pressure taps on the casing wall, a Prandtl tube at the centerline and five thermocouples located at different radii corresponding to the area centers of five equal annular areas.

Additional fixed instrumentation consisted of eight static-pressure taps located around the periphery of the manifold (station 2) and hub and tip static-pressure taps at the trailing edge of three nozzle channels (station 3) and at the leading and trailing edges of two stator channels (stations 4 and 5). The channel static-pressure taps were positioned 1/16 inch upstream of the blade trailing edge (stations 3 and 5) and 1/16 inch downstream of the blade leading edge (station 4). These static taps were located in an estimated stream tube traced through the turbine. Five wall static-pressure taps and one fixed shielded total-pressure probe were located at station 6, one blade chord downstream of the rotor. Static pressures were also measured below the hub upstream of each rotor at a radius of 5 inches (total of four pressure taps) and behind the second rotor at nominal radii of 0, 2, and 4 inches by three shielded static-pressure probes.

In addition to the fixed instrumentation, radial surveys of total pressure, total temperature, and absolute flow angle were made at station 6 with four combination probes mounted in self-aligning actuators. In figure 8 are shown the instrumentation probes at stations 6 and 7 with a section of the exhaust pipe removed. The test hardware assembled in the test facility with all instrumentation in place is shown in figure 9.

Turbine shaft torque was determined from measurement of the dynamometer torque cell balance pressure (fig. 6), which was calibrated before and after each run. Turbine rotative speed was measured with a magnetic sensing element and a shaft-mounted 60-tooth gear and read on an electronic counter. A calibrated ASME thin-plate orifice was used for weight-flow measurement. The orifice inlet pressure was read on a precision Bourdon tube gage. All other pressures were recorded simultaneously by photographing

a bank of mercury manometers. Temperatures were read on a direct-reading potentiometer. Radial position and angle of the actuated probes at station 6 were read on a calibrated-probe-position instrument supplied as part of the actuator control equipment.

EXPERIMENTAL PROCEDURE

The turbine was operated at an inlet total pressure of approximately 30 inches of mercury absolute and an inlet temperature of 550° R at equivalent nominal inlet total- to exit static-pressure ratios of 1.3, 1.55, 1.75, 1.9, 2.2, and 2.8. At each pressure ratio up to 2.2, data were taken at 60, 80, 90, 100, and 110 percent of equivalent design speed. At the highest pressure ratio, data were taken only at 100 and 110 percent of equivalent design speed. Zero-speed torque data were taken over a pressure ratio range of 1.3 to 2.3.

At design equivalent speed and pressure ratio, survey data were taken at station 6 with the four actuated combination probes at each of nine radial positions between the hub and the tip. The actuated probes were positioned at the mean radius for all other turbine operating conditions. The turbine tare torque was measured by motoring the test unit, with the rotors removed, over the range of speeds investigated and was less than 1 percent of the turbine output.

DATA REDUCTION

The turbine specific work was calculated from weight-flow, speed, and torque measurements. The torque value used was the sum of the torque indicated by the pneumatic torque cell and the test unit tare torque.

The overall turbine performance was based on the ratio of calculated inlet total pressure at station 1 to the average value of measured wall static pressure at station 7 $p_1'/\bar{p}_{7,w}$. The inlet total pressure was calculated from the average of the eight static pressure readings in the feedpipes, the total feedpipe flow area, the average inlet total temperature, and the weight flow in the same manner as in reference 2. Calculated values of total pressure averaged 0.5 percent below the measured values at the center of the feedpipes (station 1).

The measuring stations used to rate the turbine did not coincide with the stations used in the design of the turbine; therefore, a new set of design point parameters was calculated. The design pressure ratio given in reference 1 was based on the conditions at the planes of the leading edge of the nozzle and the trailing edge of the second rotor, whereas the experimental investigation included the flow processes in the feedpipes and

the manifold and in a segment of the exhaust pipe. Station 1 was selected as the inlet rating station for the investigation reported herein because of the large variation of flow conditions within the manifold (ref. 2). Station 7 was used as the downstream rating station because it was the closest constant-section plenum to the turbine exit. The design total- to static-pressure ratio for the combustion products of hydrogen and oxygen corresponding to these new rating stations was calculated by use of the following equation:

$$\frac{p_1'}{p_{7,w}} = \left(\frac{p_1'}{p_2'}\right) \left(\frac{p_2'}{p_{6,m}}\right) \left(\frac{p_{6,m}}{p_{6,t}}\right) \left(\frac{\bar{p}_{6,t}}{\bar{p}_{7,w}}\right) = \left(\frac{208.1}{200}\right) (1.667) \left(\frac{120}{124.4}\right) (1.039) = 1.738$$

This value of 1.738 was then corrected to an equivalent pressure ratio value for standard air of 1.745 by the method of reference 2. The ratio $\bar{p}_{6,t}/\bar{p}_{7,w}$ was measured during the testing; the remaining ratios in this equation are design values given in reference 1. With this new value of design pressure ratio, the design static efficiency and blade-jet speed ratio inclusive of the inlet manifold were calculated to be 0.536 and 0.128, respectively (table I, p. 5).

RESULTS AND DISCUSSION

This section contains three parts. The initial part presents the overall turbine performance calculated from weight flow, torque, speed, and pressure measurements. Following this part is a description of the flow conditions in the feedpipes, inlet manifold, and turbine as determined from static-pressure measurements. The last part presents the results of the radial surveys made at the turbine exit of total pressure, absolute flow angle, and temperature.

Overall Performance

The overall turbine performance as rated between measuring stations 1 and 7 is presented in figures 10 to 14. The performance data were obtained by use of air at ambient inlet conditions and were reduced to equivalent parameters.

Specific work. - The variation of turbine equivalent specific work with total- to static-pressure ratio is shown in figure 10 for speeds from 60 to 110 percent of design speed. The design point in this figure, as in all subsequent performance figures, is indicated by a solid circle. The specific work increased with pressure ratio and speed over the ranges investigated.

At the equivalent design speed and pressure ratio (1.745), the turbine equivalent

specific work was 9.61 Btu per pound, which was 2.3 percent less than the design value of 9.832 Btu per pound. At equivalent design speed, the design value of specific work was obtained at a pressure ratio of 1.787.

Pressure ratios across the turbine great enough to achieve limiting loading were not obtainable. Limiting loading was being approached, however, as evidenced by the decreasing slope of the curves, particularly for 100 and 110 percent of equivalent design speed, with increasing pressure ratio.

Overall static efficiency. - The variation of static efficiency with percent equivalent design speed and equivalent total- to static-pressure ratio is presented in figure 11. The static efficiency at any given speed decreased with increasing turbine pressure ratio. At the equivalent design speed and pressure ratio, the static efficiency was 0.524, which was 2.2 percent lower than the design value of 0.536.

The static efficiency variation with blade-jet speed ratio and rotative speed is shown in figure 12. The static efficiency increased with increasing blade-jet speed ratio with the peak efficiency indicated at a value of blade-jet speed ratio higher than the range investigated. An examination of this figure reveals the presence of a family of curves with percent equivalent design speed as the parameter. At any given rotor speed and at the higher pressure ratios tested (lower blade-jet speed ratios), the efficiency curve becomes tangent to an envelope curve. At the lower pressure ratios tested, the efficiency falls below the envelope curve for each speed.

Weight flow. - The variation in equivalent weight flow with equivalent pressure ratio for the equivalent speeds investigated is shown in figure 13. In general, the equivalent weight flow increased with pressure ratio for all speeds investigated. Also, at all but the maximum pressure ratio investigated, the weight flow decreased with increasing speed. At equivalent design speed and pressure ratio, the measured equivalent weight flow was 6.31 pounds per second, which is 10.8 percent below the design weight flow of 7.071 pounds per second. A weight-flow deficiency of 10.2 percent was measured during the manifold tests (ref. 2), where it was concluded that the undersize nozzle-throat area (3.7 percent) and unfavorable manifold flow conditions were responsible.

A nearly choked equivalent weight flow of 6.57 pounds per second was approached at an equivalent total- to static-pressure ratio of about 2.8. This value of weight flow compares well with the maximum value (6.55 lb/sec) measured in the prior manifold tests. The convergence of the speed lines at this pressure ratio indicates that the nozzle is approaching a choked flow condition prior to any other blade row.

Torque. - The variation in equivalent torque with percent equivalent speed is shown in figure 14 for the range of equivalent pressure ratios investigated. The torque continually decreased with speed for all pressure ratios covered. At any given speed, the torque increased with increasing pressure ratio. The measured equivalent torque at design equivalent speed and pressure ratio was 238 foot-pounds, which was 12.8 percent

lower than the design value of 273 foot-pounds. This deficiency in torque, and therefore power, at equivalent design speed and pressure ratio is the net result of the deviations of weight flow and specific work from their design values. At design pressure ratio, the ratio of starting torque to torque at design speed is approximately 1.3.

Static-Pressure Distribution

Static pressures measured in the feedpipes, inlet manifold, and stator channels are plotted in figures 15 to 17. These measurements were used to investigate the flow conditions in the turbine and are discussed in the succeeding paragraphs. In addition, rotor-hub static pressures are presented to assist in evaluating the shaft axial thrust characteristics.

Inlet conditions. - The variation in feedpipe static- to total-pressure ratio with turbine-inlet total- to turbine-exit static-pressure ratio at equivalent design speed is shown in figure 15(a). The static pressure \bar{p}_1 is the average of the four wall taps in each feedpipe, and the total pressure $p'_{1,t}$ is the measured value at the center of each feedpipe.

The flow characteristics of the two feedpipes are quite different. The flow conditions in the left feedpipe do not change above turbine pressure ratios of approximately 1.8, whereas the flow conditions in the right feedpipe continue to change up to the highest pressure ratio investigated. This difference implies that above design pressure ratio the weight flow through the left feedpipe is constant and that any increase in flow must come from the right feedpipe. At the turbine design pressure ratio, the computed Mach numbers for the right and left feedpipes were 0.25 and 0.32, respectively, which indicated that approximately 44.5 percent of the total weight flow passed through the right feedpipe and 55.5 percent through the left feedpipe. These differences in feedpipe flow conditions are attributed to the different flow and loss mechanisms on either side of the manifold. For example, nozzle incidence on the right side of the manifold is positive, whereas the incidence on the left side is negative. A larger effective blockage may thus be created on the right half of the manifold. The manifold tests (ref. 2) had indicated larger losses on the right half than on the left half of the manifold.

Figure 15(b) is a cross plot of data showing the manifold static pressure circumferential variation for several values of turbine pressure ratio at equivalent design speed. The static-pressure variation shown is very similar to that measured in prior manifold tests (ref. 2), where sizable variations in flow velocities were concluded to exist around the manifold periphery. The highest velocities prevailed in the vicinity of the feedpipes, as expected from geometric considerations, and lower velocities existed between feedpipes at the manifold top and bottom. As turbine pressure ratio was increased, the

static- to inlet total-pressure ratio decreased, as expected, inasmuch as the equivalent weight flow continuously increased (fig. 13). The relatively small change in static pressure as the turbine pressure ratio was increased from 2.1 to 2.8 indicates the near approach to choking conditions, as mentioned previously. No change occurred in the region of the left feedpipe, where the flow was constant (fig. 15(a)), whereas in the region of the right feedpipe, small changes occurred as affected by the slight increase in flow through this feedpipe.

Flow path static pressures. - The axial static-pressure distribution at the hub and the tip of the blades measured at equivalent design speed and pressure ratio is shown in figure 16(a). The average of the static pressures measured at each station (maximum circumferential variation, ± 2.7 percent) is divided by the calculated inlet total pressure. The resulting values are connected with straight lines to define the hub and the tip readings. The design static-pressure distribution is shown by a dashed line. In general, the level of static pressures within the turbine shows reasonable agreement with the design values; the tip values are in better agreement than the hub values. A meaningful comparison between the measured and the design static pressures, however, cannot be made because of the undersized and mismatched throat areas of the test hardware. The first-stage rotor, for example, was designed to have a constant static pressure at the mean section. Measurements indicated a small static-pressure decrease through this blade row, but this decrease may have been caused by the undersize throat areas.

One obvious feature noted in the data of figure 16(a) is the almost complete lack of a radial pressure gradient from hub to tip. This condition is quite different from both the design pressure distribution and the static pressures recorded at station 3 during the manifold tests (ref. 2), when the rotors and stator were removed. The latter pressure measurements taken at the design nozzle-mean-exit static- to inlet total-pressure ratio $p_{3,m}/p_1'$ are shown by triangular symbols. Also, the nozzle design pressure ratio $\bar{p}_{3,m}/\bar{p}_1'$ of 0.607 was not obtained at the overall design pressure ratio $p_1'/\bar{p}_{7,w}$ of 1.745 of the turbine. This difference in nozzle pressure ratio between the manifold and the two-stage tests accounts for the small change in measured weight flow previously mentioned.

Shown in figures 16(b) and (c) are the results of cross plots of the circumferentially averaged axial static-pressure distribution at the tip and the hub, respectively, of the stators at design speed for a range of turbine pressure ratios. This figure is useful in determining the choking characteristics of the turbine hardware tested. As stated previously, the turbine weight flow measurements (fig. 13) indicated that the nozzle was operating very nearly choked at the maximum pressure ratio. This flow condition is also indicated in figures 16(b) and (c) by the almost constant value of static pressure at the nozzle exit (station 3) at the higher overall pressure ratios. As the nozzle approaches choked conditions, the velocity diagrams (fig. 2) imply that the first-stage rotor also approaches choked

flow at the blade leading edge. The axial static-pressure data also indicate that the second-stage stator and rotor were not choked over the range of pressure ratios investigated.

Disk-face static pressures. - The static pressures measured on each side of the rotor disks are plotted in figure 17. Figure 17(a) shows the comparison between design and measured radial static-pressure gradient in the flow path and below the rotor hub at equivalent design speed and pressure ratio. The design static pressure distribution is shown by dashed lines. At measuring stations 3, 4, and 5 there is little radial variation in static pressure from the blade tip to points below the hub, as mentioned previously. The pressures at and below the hub at station 3, however, are higher than the hub design static pressure, whereas the static pressures measured at station 6 below the hub are considerably below design. The net result of these static-pressure changes from design is a significantly larger shaft thrust than expected directed toward the turbine exit.

Figure 17(b) shows the measured variation of the static pressure acting on the faces of both rotor disks at five equivalent pressure ratios for each of five speeds. The cross-plotted pressure ratios p/p_1^* at different measuring stations are connected by straight lines to identify the readings taken at a given turbine pressure ratio $p_1^*/\bar{p}_{7,w}$. The local static- to inlet total-pressure ratios indicated for measuring station 6 (downstream of the second-stage rotor) are the average of the three radial stations shown in figure 17(a). The data presented in figure 17(b) can be used to evaluate the variation in shaft thrust at off-design operation. The static pressures measured at stations 3 and 6 indicate that the shaft thrust increases directly with overall pressure ratios and is always directed toward the turbine exit for all rotor speeds investigated. At any given pressure ratio, there are only minor changes in axial thrust with a change in rotative speed.

Turbine-Exit Surveys

The results of the radial survey (station 6) of total pressure, absolute flow angle, and temperature taken at equivalent design speed and pressure ratio are shown in figure 18. The design flow conditions taken from reference 1 are shown for comparison and are indicated by dashed lines.

Total-pressure survey. - Figure 18(a) presents the total-pressure measurements taken at the turbine exit, which show that the total pressure varied circumferentially as well as radially. The radial variation was virtually the inverse of the design variation. Losses lower than design (higher total pressures) occurred between the hub and the mean section, while losses larger than design occurred at the tip section.

The circumferential variation in total pressure is attributed to the flow conditions in the manifold. The highest nozzle-inlet total pressures were recorded (ref. 2) in line with the feedpipes, while the lowest pressures were recorded adjacent to the feedpipes,

with smaller pressure variations recorded around the remainder of the circumference. Position B (fig. 18(a)) was in line with the left feedpipe. Positions A and D were in the low-pressure areas on either side of the feedpipes, whereas position C was removed from either the high- or the low-pressure areas. The maximum circumferential total-pressure variation at the mean diameter of the turbine exit was only 2.1 percent, about one-fifth that measured at the nozzle inlet. The large variation in nozzle-inlet total pressure was apparently attenuated in passing through the turbine.

Angle survey. - The variation in absolute flow angle with location is shown in figure 18(b). The flow at the turbine exit is overturned for all but the tip region of the blade passage and exhibits considerable variation circumferentially. The amount of overturning was as large as 10° ; this amount occurred midway between the blade hub and mean sections on the right side of the manifold (position D). At the blade tip, the flow is markedly underturned at all circumferential locations. Calculations made by use of the total- and static-pressure values at the tip of the turbine exit indicated that the absolute Mach number was lower than design. The Mach number varied from about 0.150 to 0.215, as compared with the design value of 0.274. These low velocities account for the underturning of the flow at the blade tip.

Temperature survey. - The results of the total-temperature survey at the turbine exit are shown in figure 18(c). The survey indicated gas temperatures slightly lower than design; higher specific work was thus indicated than that calculated from the torque, weight-flow, and speed measurements. The difference between the two methods of calculating the specific work, however, is of the order of only 2 percent and is probably caused by the inaccuracy inherent in the use of gas temperatures. The enthalpy drop across the turbine (indicated by $1 - (T_6'/T_1')$) varied by as much as 13 percent from hub to tip, with the flow in the vicinity of the hub and tip doing less work per pound than the remaining flow stream.

SUMMARY OF RESULTS

The aerodynamic performance of a 0.45-scale oxidizer pump-drive turbine including its inlet-manifold assembly for the M-1 rocket engine was determined with air at ambient inlet conditions. Speed was varied from 60 to 110 percent of equivalent design speed for equivalent pressure ratios ranging from 1.3 to 2.8. The results of the investigation are summarized as follows:

1. At equivalent design speed and overall total- to static-pressure ratio, the static efficiency was 0.524 and the equivalent specific work was 9.61 Btu per pound. The corresponding design values were 0.536 and 9.832 Btu per pound, respectively.
2. The equivalent weight flow measured at design speed and pressure ratio was 6.31

pounds per second, which is 10.8 percent below the design value of 7.071 pounds per second. Of this deficiency, 3.7 percent is attributed to the undersize nozzle-throat area of the test hardware, with the remaining part charged to adverse flow conditions in the inlet manifold and nozzle channels.

3. The result of lower efficiency and weight flow than design was a net loss in turbine power of 12.8 percent at design equivalent speed and pressure ratio.

4. Static pressures measured at the blade tip and hub and below the hub showed that

(a) Only small radial gradients existed at all axial stations through the turbine except at the turbine exit.

(b) The turbine shaft thrust was appreciably higher than predicted.

5. A radial survey made at the turbine exit at four circumferential locations at design equivalent speed and pressure ratio revealed that

(a) The pattern of circumferential and radial variations in nozzle-inlet total pressure measured in prior manifold tests persisted through the turbine but the magnitude of the variations was diminished.

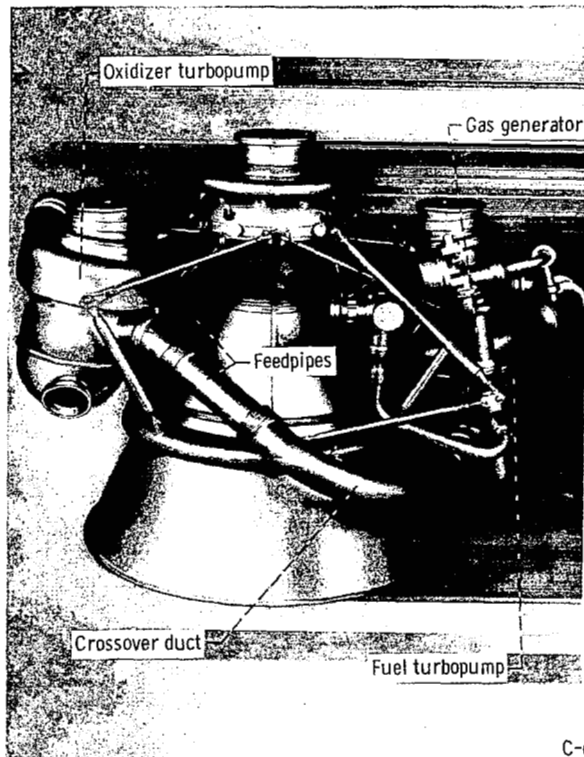
(b) A considerable circumferential variation in flow angle existed. Overturning of the flow occurred at all but the tip region of the blade passage. At the blade tip, flow velocities were lower than design and the flow was significantly underturned.

(c) Total-temperature measurement indicated significant variations in the enthalpy drop across the turbine from hub to tip.

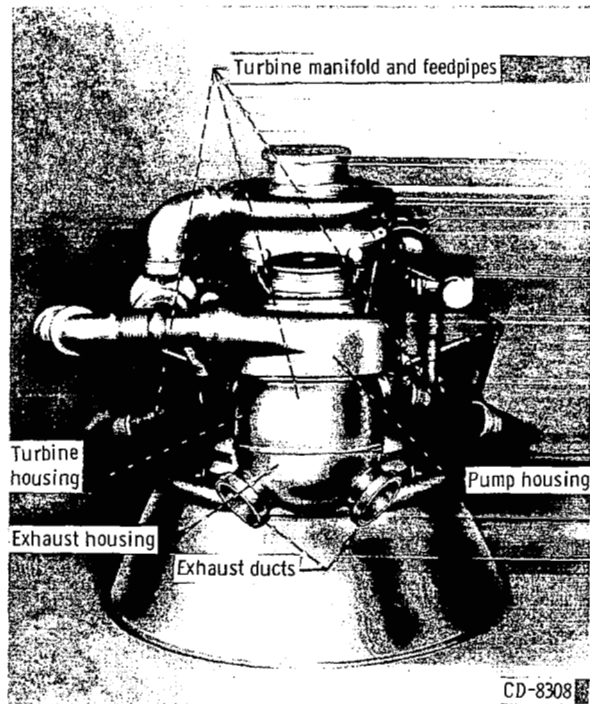
Lewis Research Center,
National Aeronautics and Space Administration,
Cleveland, Ohio, December 6, 1965.

REFERENCES

1. Beer, R. : Aerodynamic Design and Estimated Performance of a Two-Stage Curtis Turbine for the Liquid Oxygen Turbopump of the M-1 Engine. Rept. AGC-8800-12, Aerojet General Corp. (NASA CR-54764), 1965.
2. Stabe, Roy G. ; Evans, David G. ; and Roelke, Richard J. : Cold-Air Performance Evaluation of Scale Model Oxidizer Pump-Drive Turbine for the M-1 Hydrogen-Oxygen Rocket Engine. I - Inlet Feedpipe-Manifold Assembly. NASA TN D-3294, 1966.
3. Holeski, D. E. ; and Stewart, W. L. : Study of NASA and NACA Single-Stage Axial Flow Turbine Performance as Related to Reynolds Number and Geometry. J. Eng. Power, vol. 86, no. 3, July 1964, pp. 296-298.

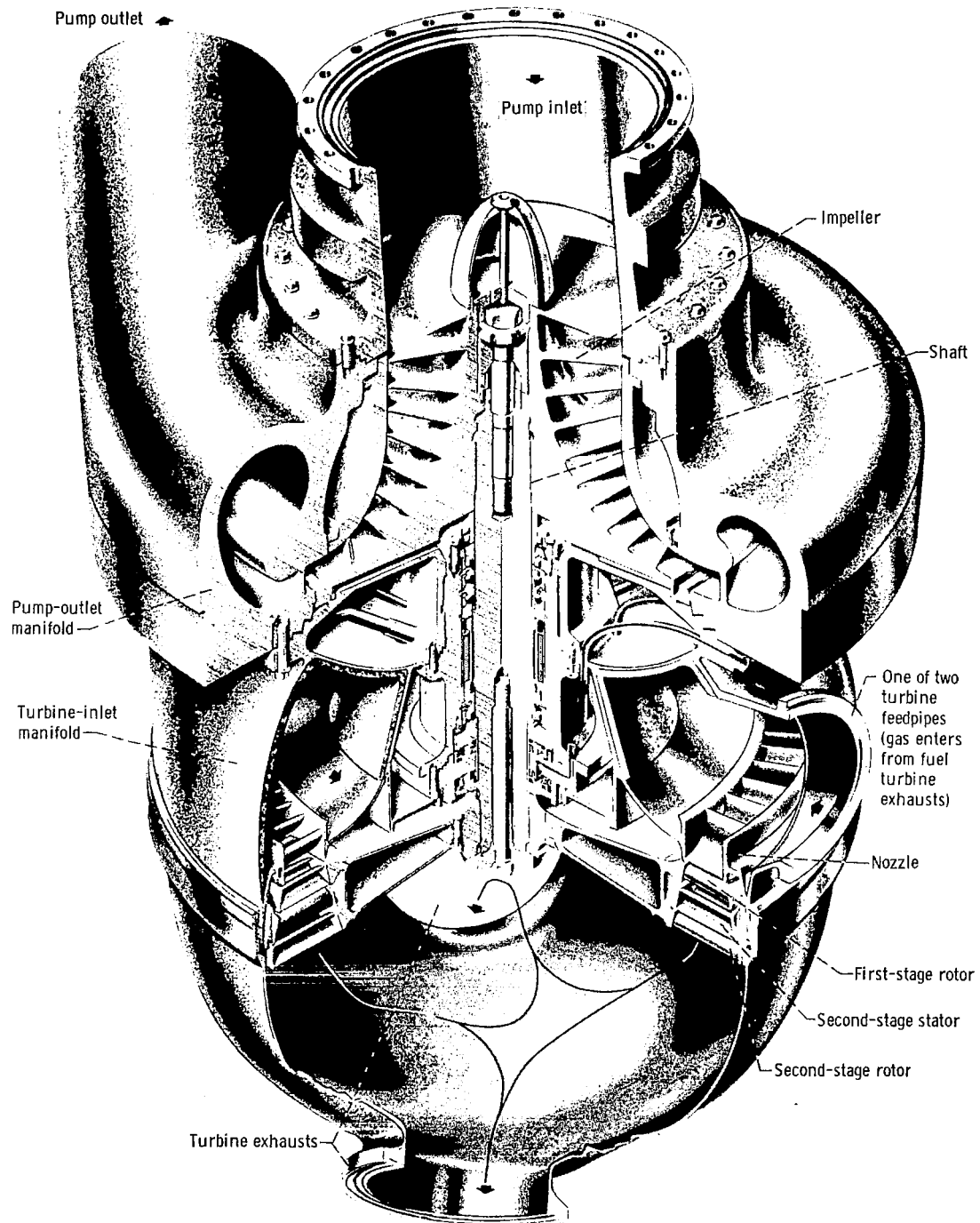


(a) Side view of turbopump.



(b) Oxidizer turbopump.

Figure 1. - Mockup of M-1 hydrogen-oxygen rocket engine Model III turbomachinery mounted on combustion chamber.



CD-8282

Figure 2. - Oxidizer turbopump assembly.

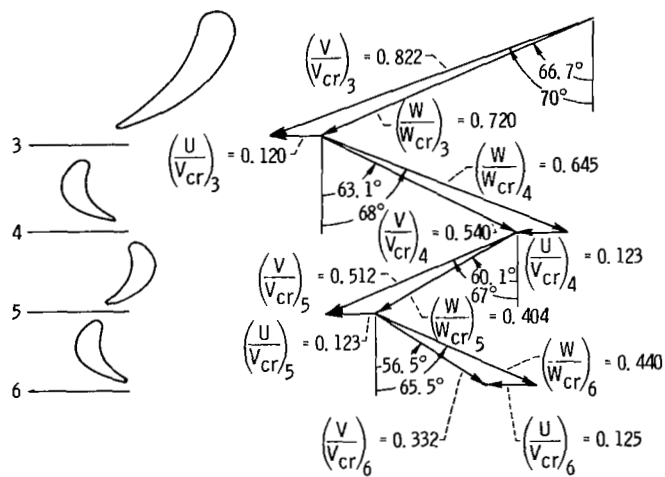


Figure 3. - Design free-stream velocity diagrams at mean diameter.

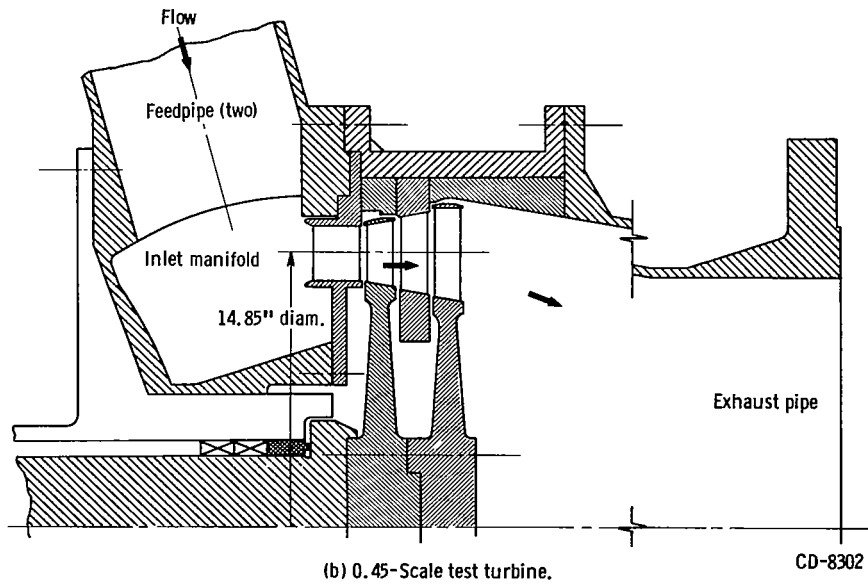
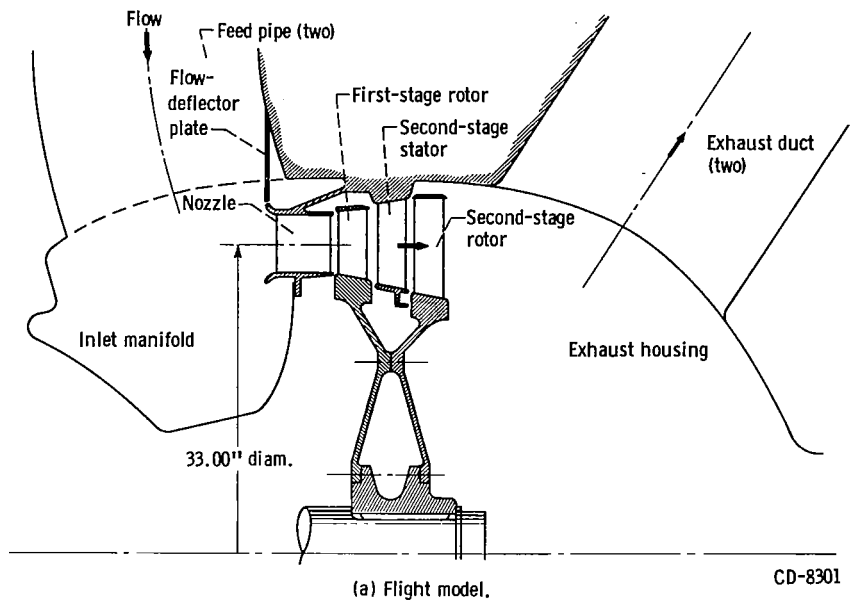
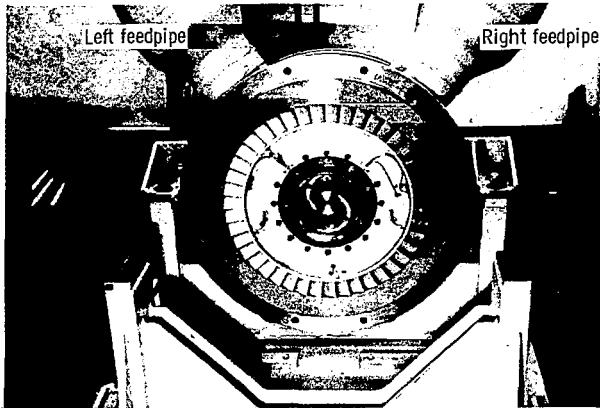
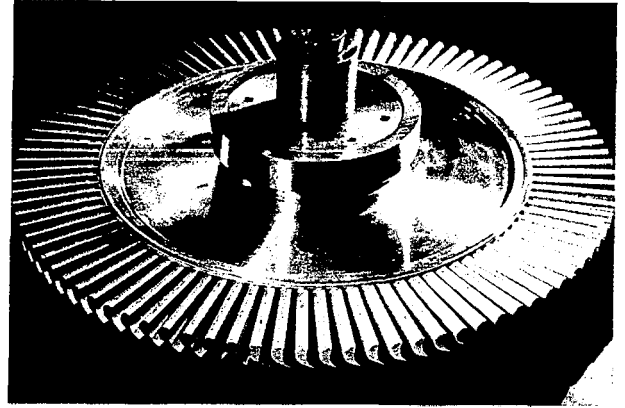


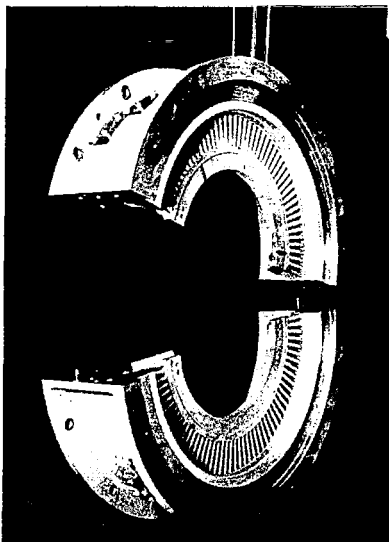
Figure 4. - Cross section of Model III oxidizer turbine.



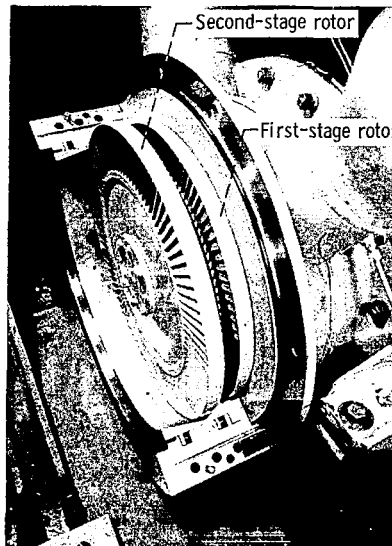
(a) Nozzle installed in manifold-feedpipe assembly.



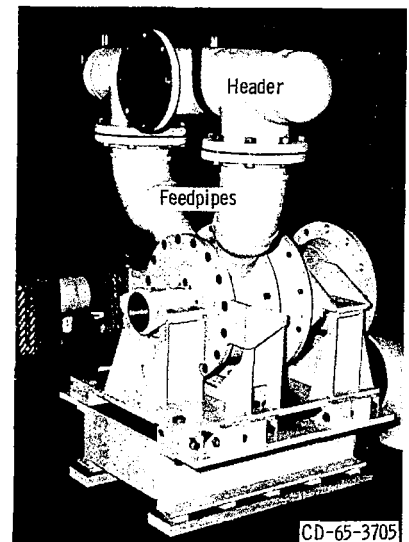
(b) Second-stage rotor prior to installation of tip shroud.



(c) Split casing halves with second-stage stator installed.



(d) Rotors installed on turbine shaft.



(e) Header, feedpipes, and turbine support stand.

Figure 5. - Test turbine hardware.

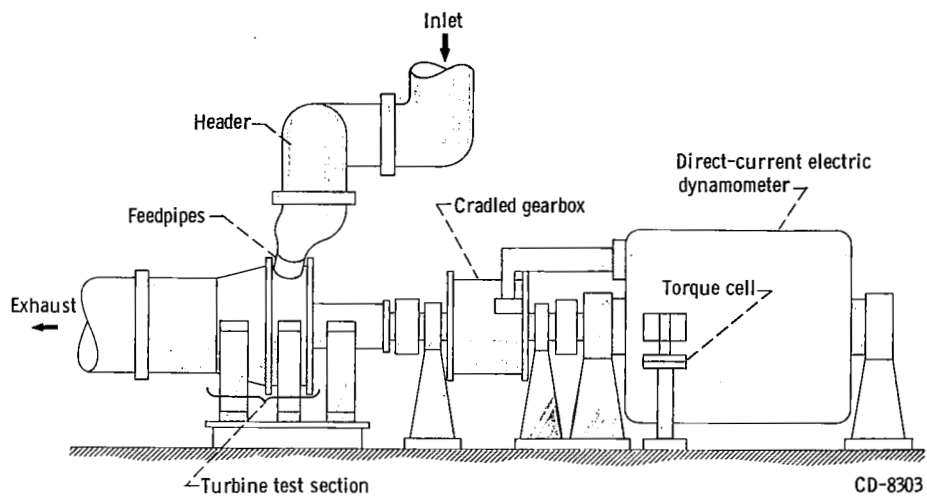


Figure 6. - Test facility.

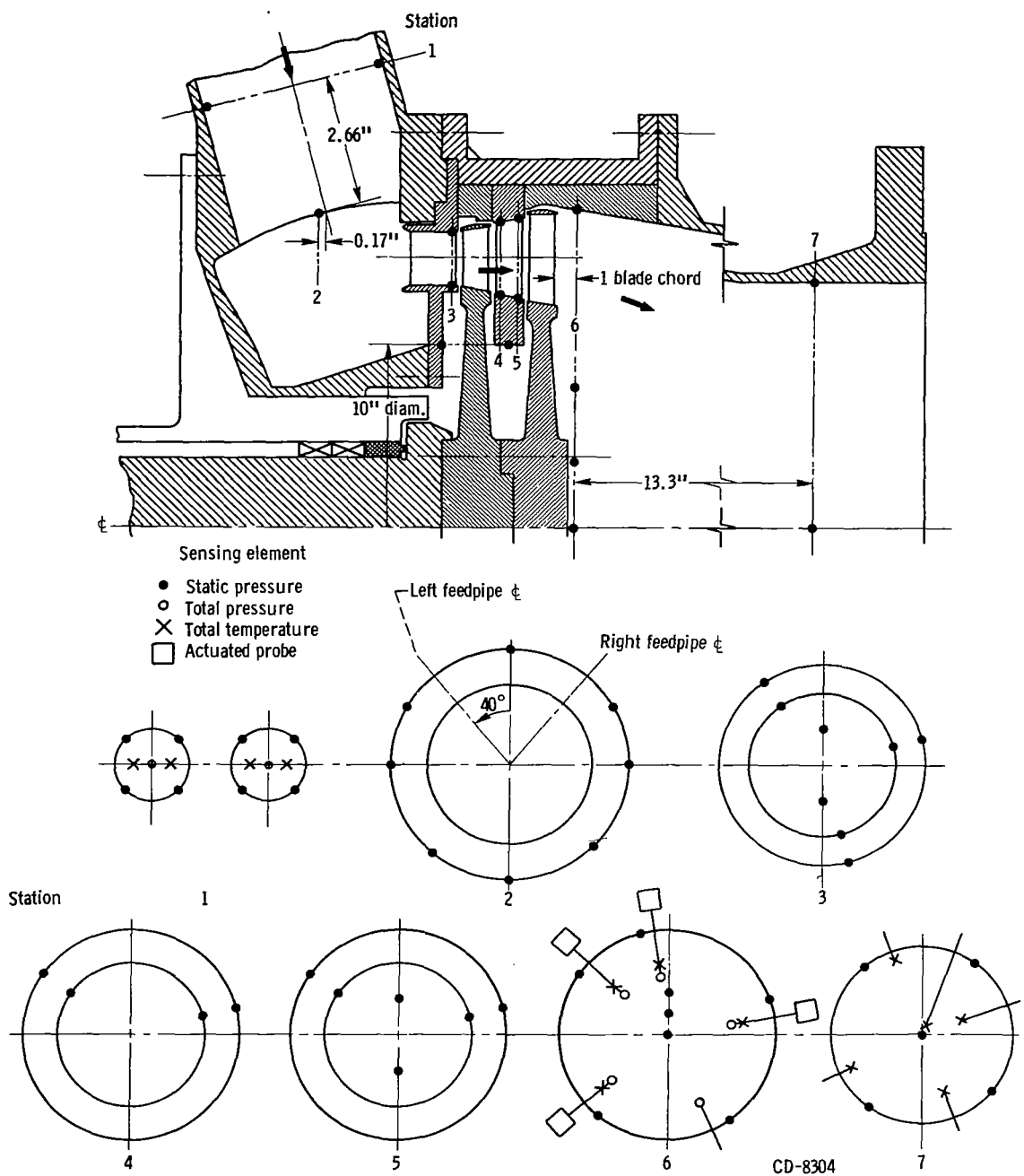


Figure 7. - Test turbine instrumentation.

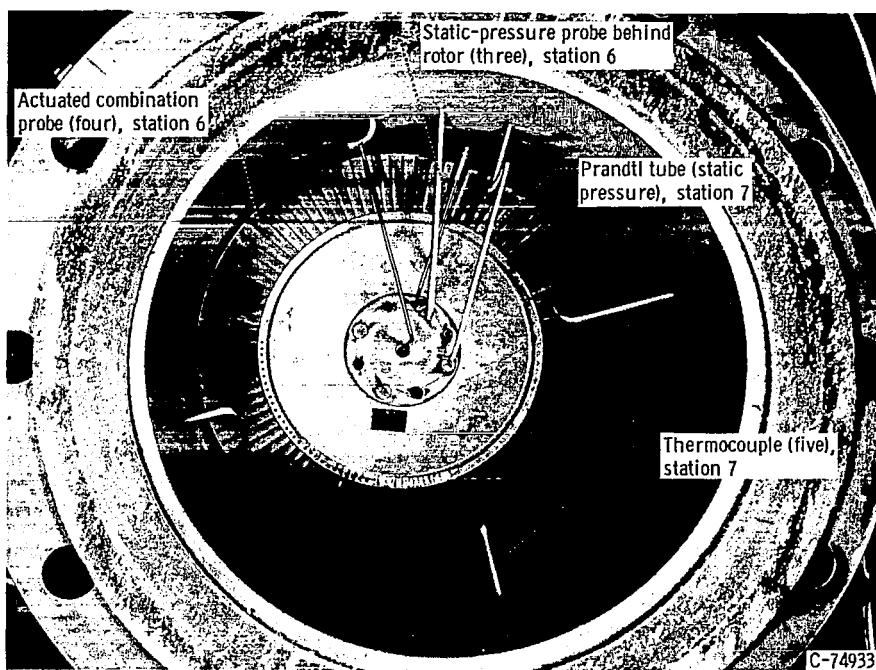


Figure 8. - Instrument probes in turbine-exhaust pipe, stations 6 and 7.

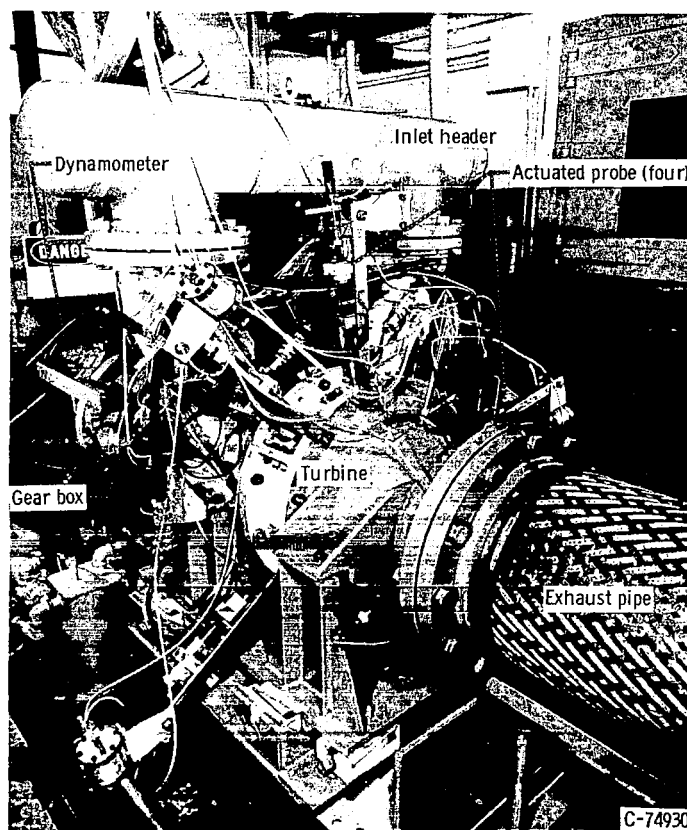


Figure 9. - Test turbine assembled and instrumented in test cell.

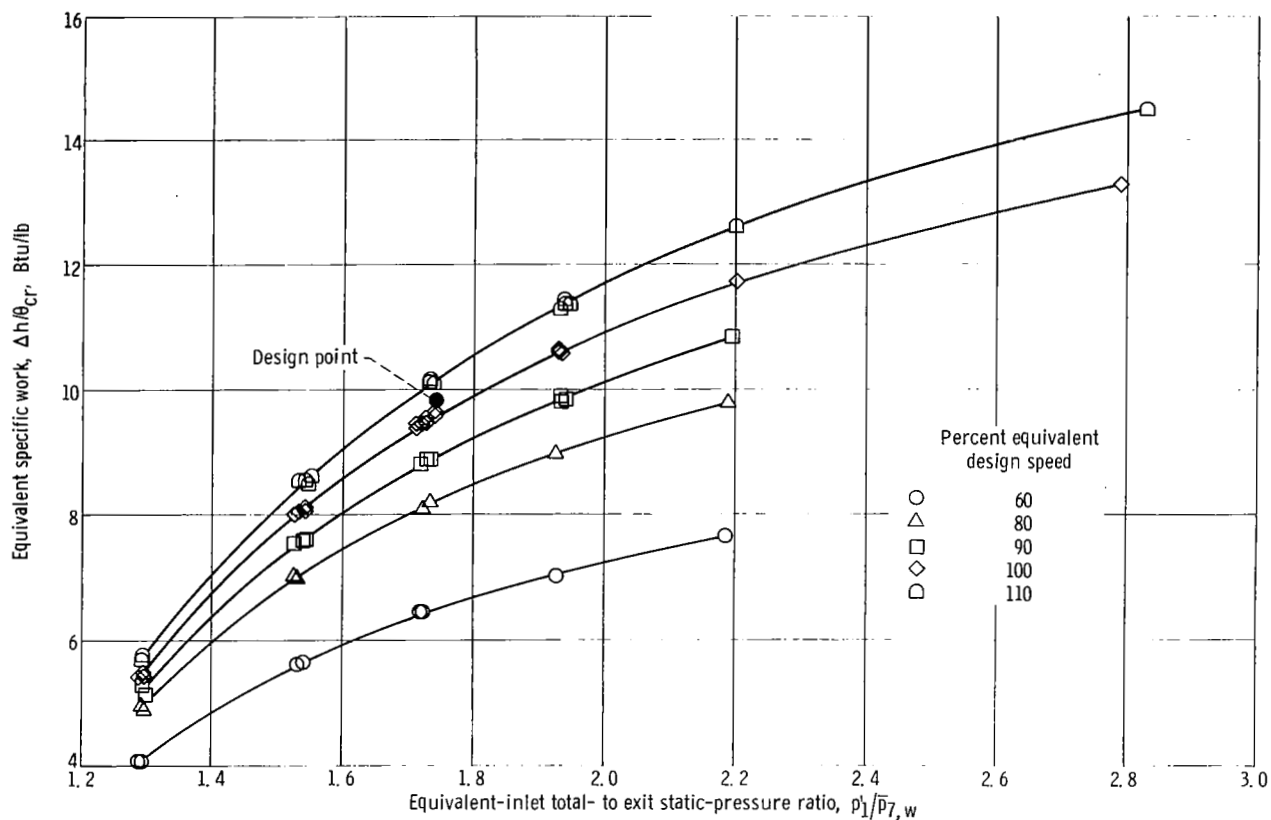


Figure 10. - Variation of equivalent specific work with percent equivalent design speed and pressure ratio.

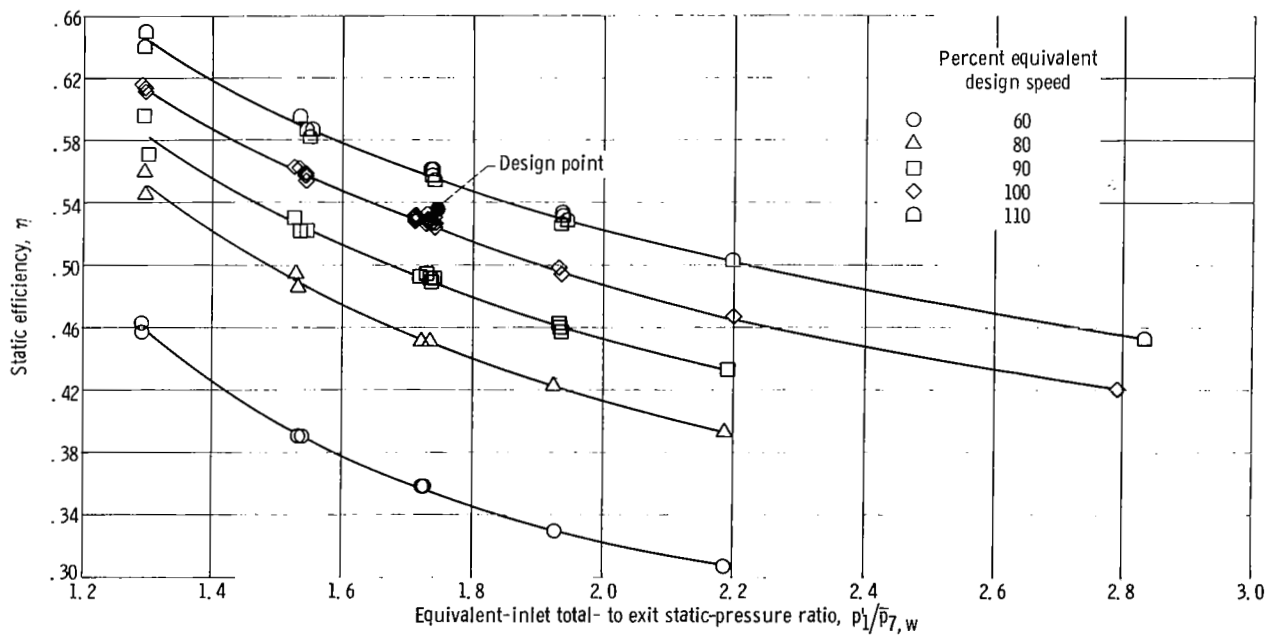


Figure 11. - Variation of static efficiency with percent equivalent design speed and pressure ratio.

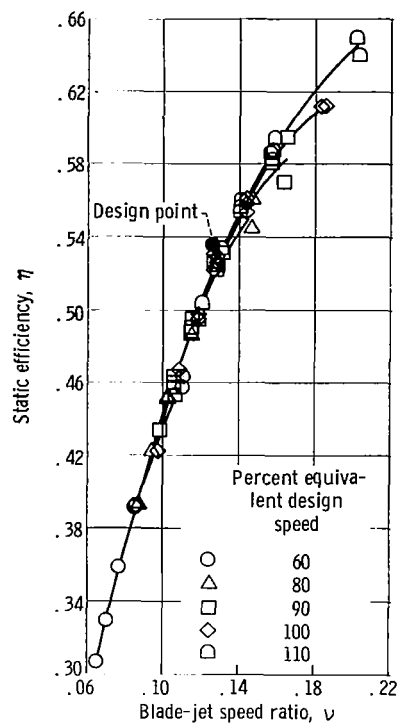


Figure 12. - Variation of static efficiency with blade-jet speed ratio and percent equivalent design speed.

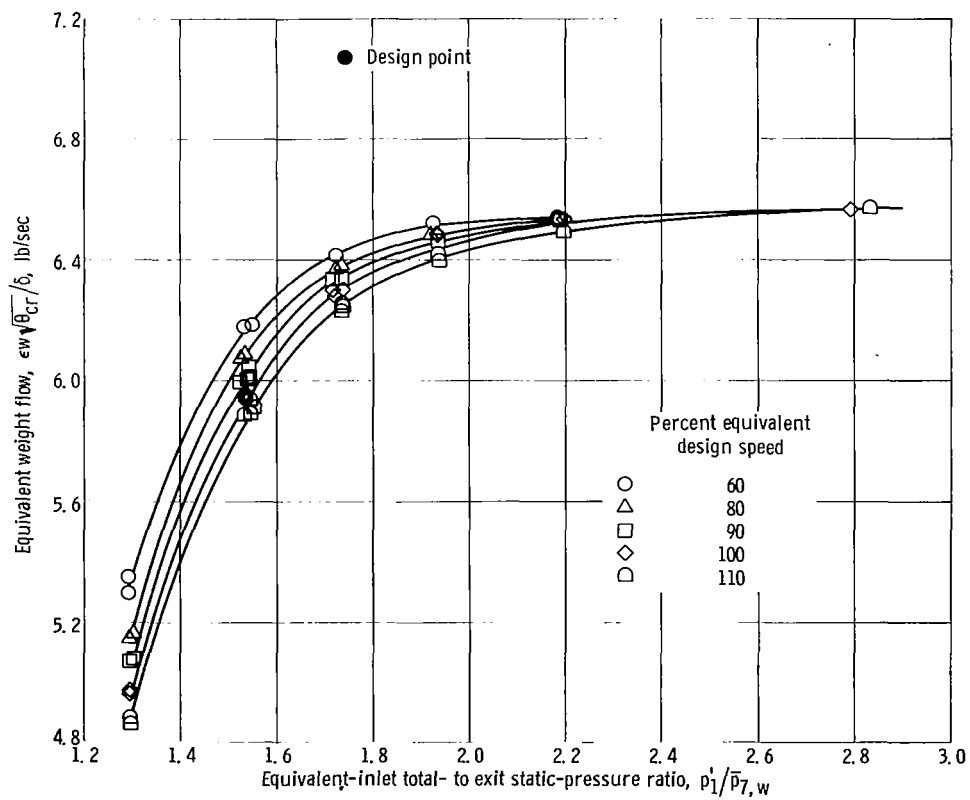


Figure 13. - Variation of equivalent weight flow with percent equivalent design speed and pressure ratio.

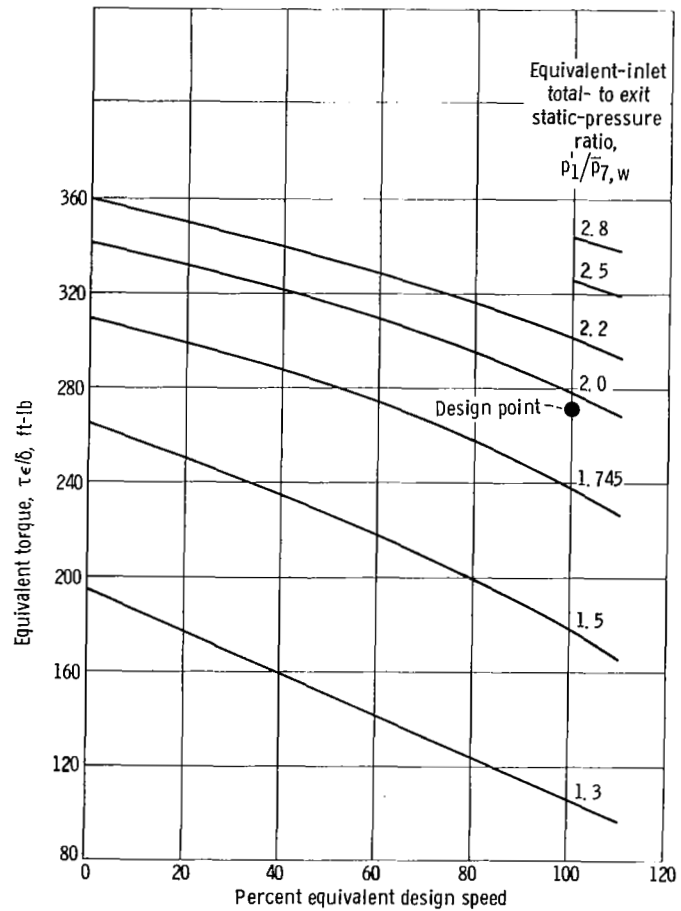
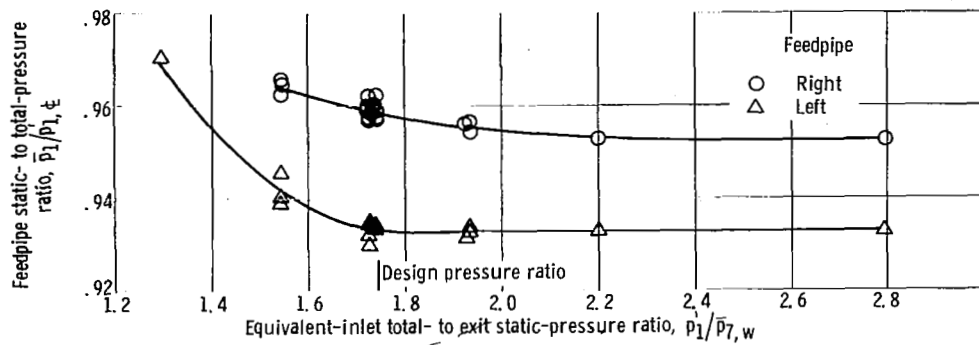
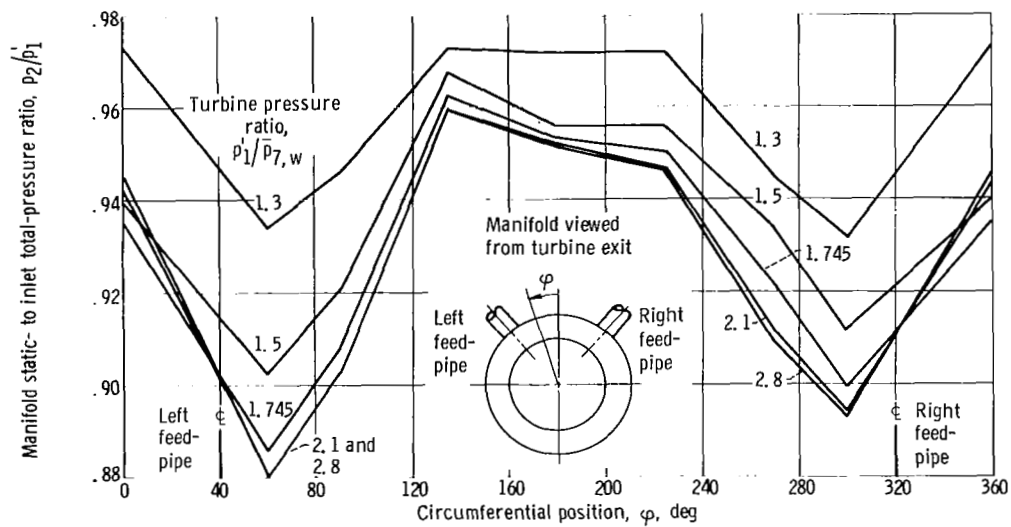


Figure 14. - Variation of equivalent torque with percent equivalent design speed and pressure ratio.

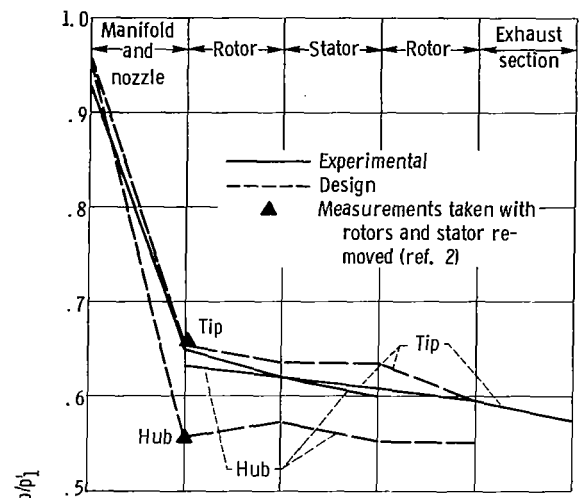


(a) Variation in feedpipe static- to total-pressure ratio with turbine pressure ratio at equivalent design speed.

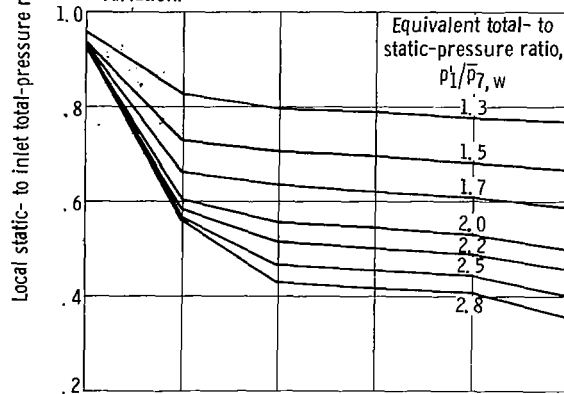


(b) Circumferential variation in manifold outer-wall static pressure with position and turbine pressure ratio at equivalent design speed.

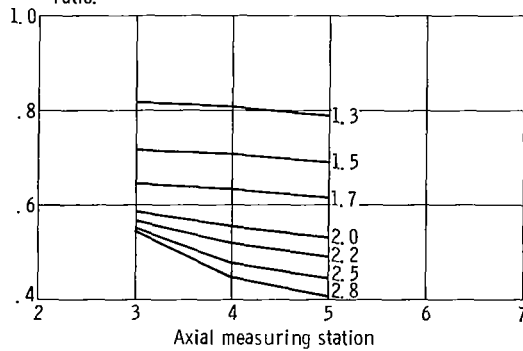
Figure 15. - Turbine-inlet pressure measurements.



(a) Comparison of design and experimental static-pressure variation.

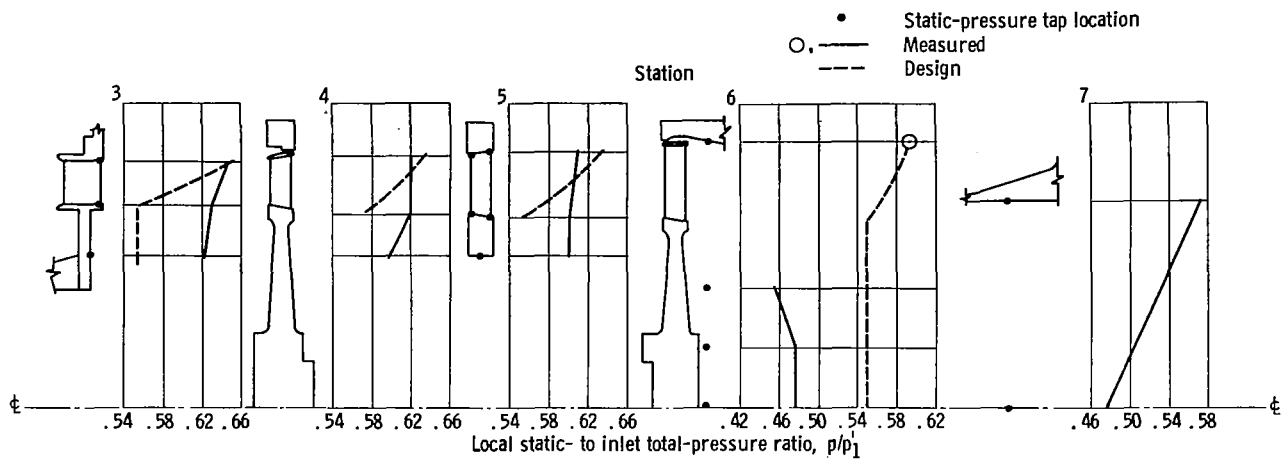


(b) Variation of tip static pressure with turbine pressure ratio.

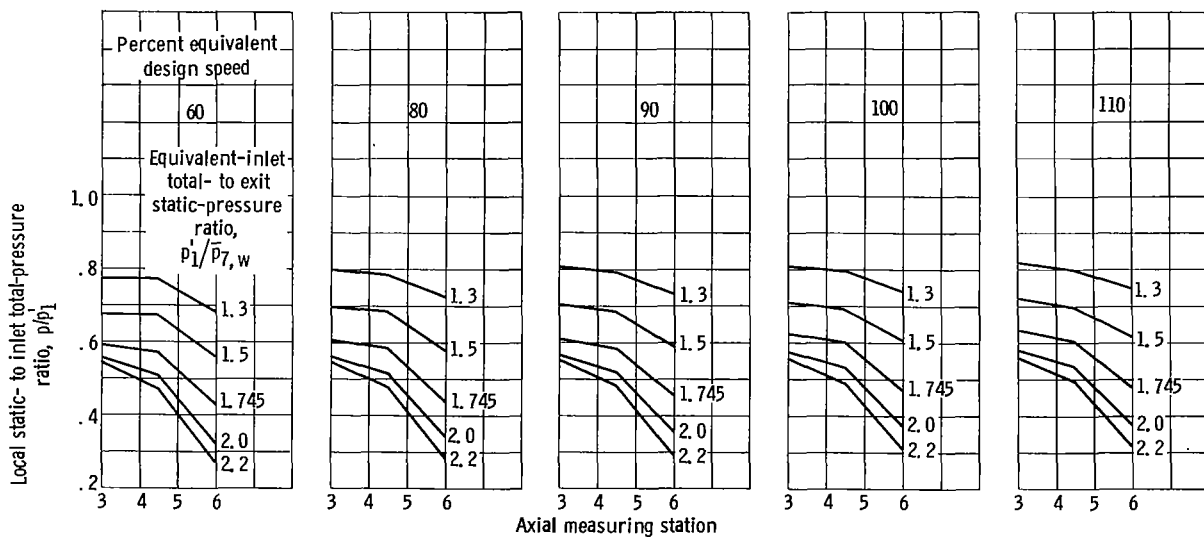


(c) Variation of hub static pressure with turbine pressure ratio.

Figure 16. - Flow passage static pressures at equivalent design speed.



(a) Comparison of design and measured radial variation across flow path and disk faces at equivalent design speed and pressure ratio.



(b) Variation of static pressures below blade hub with percent equivalent design speed and pressure ratio.

Figure 17. - Disk-face static pressures.

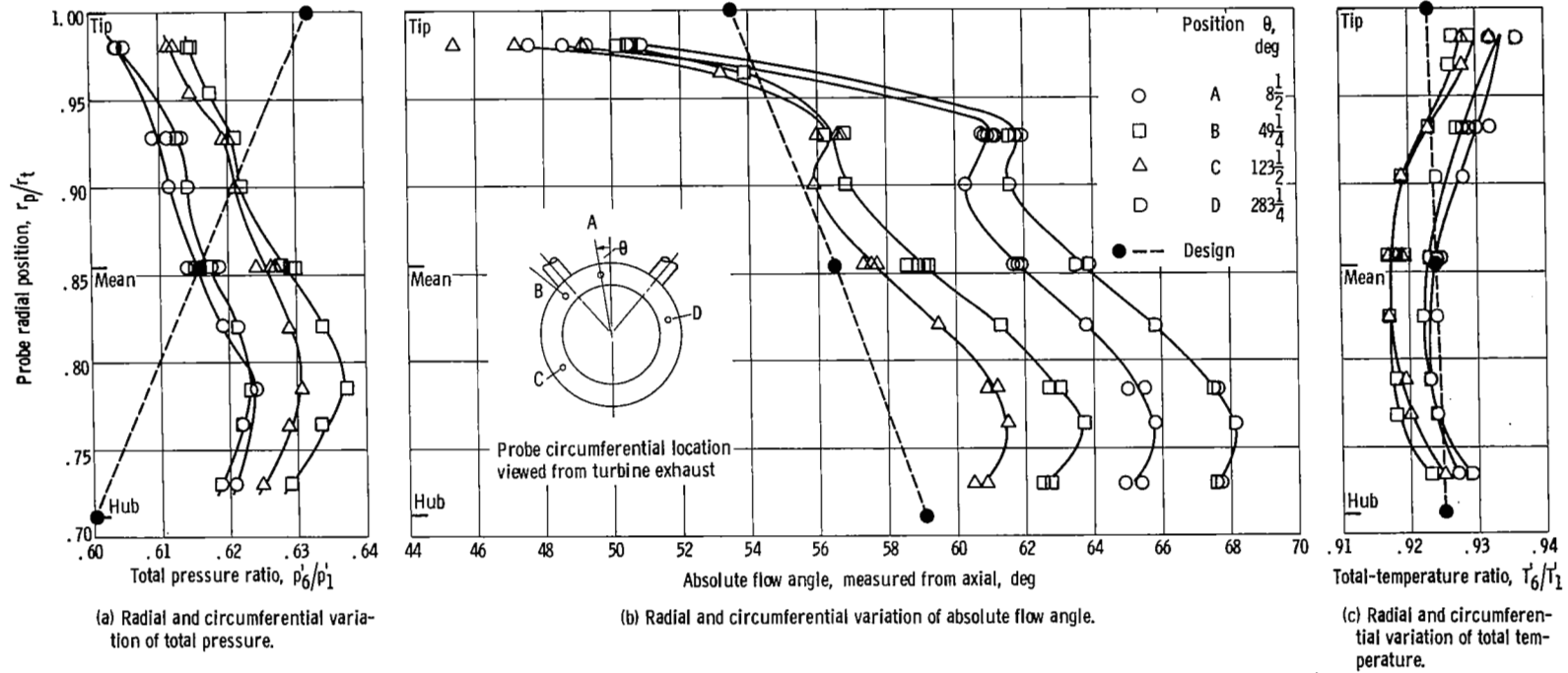


Figure 18. - Turbine-exit survey data at equivalent design speed and pressure ratio.

"The aeronautical and space activities of the United States shall be conducted so as to contribute . . . to the expansion of human knowledge of phenomena in the atmosphere and space. The Administration shall provide for the widest practicable and appropriate dissemination of information concerning its activities and the results thereof."

—NATIONAL AERONAUTICS AND SPACE ACT OF 1958

NASA SCIENTIFIC AND TECHNICAL PUBLICATIONS

TECHNICAL REPORTS: Scientific and technical information considered important, complete, and a lasting contribution to existing knowledge.

TECHNICAL NOTES: Information less broad in scope but nevertheless of importance as a contribution to existing knowledge.

TECHNICAL MEMORANDUMS: Information receiving limited distribution because of preliminary data, security classification, or other reasons.

CONTRACTOR REPORTS: Technical information generated in connection with a NASA contract or grant and released under NASA auspices.

TECHNICAL TRANSLATIONS: Information published in a foreign language considered to merit NASA distribution in English.

TECHNICAL REPRINTS: Information derived from NASA activities and initially published in the form of journal articles.

SPECIAL PUBLICATIONS: Information derived from or of value to NASA activities but not necessarily reporting the results of individual NASA-programmed scientific efforts. Publications include conference proceedings, monographs, data compilations, handbooks, sourcebooks, and special bibliographies.

Details on the availability of these publications may be obtained from:

SCIENTIFIC AND TECHNICAL INFORMATION DIVISION
NATIONAL AERONAUTICS AND SPACE ADMINISTRATION
Washington, D.C. 20546